Electronic Materials Letters (2019) 15:141–148
https://doi.org/10.1007/s13391-018-00109-4

ORIGINAL ARTICLE - CHEMISTRY AND BIOMATERIALS

Tuning of Graphene Work Function by Alkyl Chain Length in Amine-Based Compounds

Sa-Rang Bae[1] · Tae Won Lee[1] · Kwangyong Park[1] · Soo Young Kim[1]

Received: 16 November 2018 / Accepted: 26 November 2018 / Published online: 12 December 2018

Abstract

In this study, the effect of alkyl chain length in amine-based compounds on the work function of graphene was investigated. The graphene was synthesized by the chemical vapor deposition method. The graphene layers were functionalized by amine-based groups using a simple spin-coating method. The amine-based compounds were composed of phenyl amine and methyl-, ethyl-, propyl-, *n*/*t*-butyl-, and octyl-phenyl amine groups. Materials were confirmed by X-ray photoelectron spectroscopy to show the C and N bonding. The work function of the doped graphene layers decreased because of the effect of the doping agents. Among the doped graphene samples, *t*-butyl-phenyl amine functionalized graphene achieved the lowest work function of 3.89 eV (compared with 4.43 eV for pristine graphene). Further, the sheet resistance of n-doped graphene increased, confirming the high concentration of n-doping agents on the graphene layers. These results suggest the best alkyl chain is the *t*-butyl group to reduce the work function of graphene, and promise the use of these materials as cathodes for opto-electronic applications.

Graphical Abstract

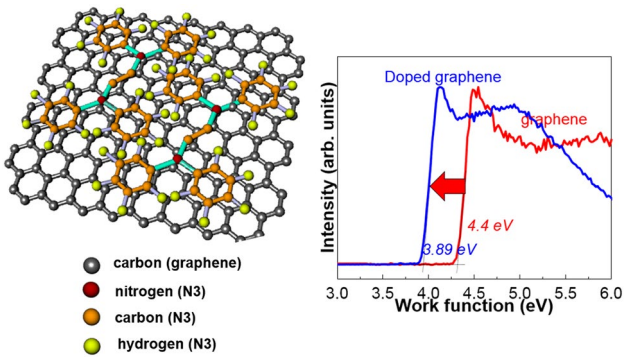

Keywords Graphene · Work function · Amine-based compounds · n-doping

1 Introduction

Graphene, an allotrope of carbon in the form of a two-dimensional, atomic-scale hexagonal lattice, has received tremendous attention in the field of electronics owing to its excellent mechanical (tensile strength of 130.5 GPa and Young's modulus of 1 TPa), thermal (5300 W m^{-1} K^{-1}), optical (absorbing $\pi\alpha \approx 2.3\%$ of red light), magnetic (1 μ_B per $\approx$ 1000 adatoms), and electrical properties (15,000 cm^2 V^{-1} s^{-1}) [1–5]. Ever since graphene was first

Sa-Rang Bae and Tae Won Lee authors contributed equally to this work.

✉ Kwangyong Park
kypark@cau.ac.kr

✉ Soo Young Kim
sooyoungkim@cau.ac.kr

[1] School of Chemical Engineering and Materials Science, Chung-Ang University, 84 Heukseok-ro, Dongjak-gu, Seoul 06974, Republic of Korea

synthesized by chemical vapor deposition (CVD), there have been many reports on the application of graphene layers to the transparent electrodes of solar cells, light-emitting diodes, field-effect transistors, touch panels, and smart windows or phones [6]. The CVD process is one of the more promising processes for synthesizing graphene with a large area, low sheet resistance (< 100 Ω/sq.), and high transparency (> 90%) [7–9].

It has been known that chemical dopants can change the ability of a semiconductor to control its work function by efficient Fermi-level engineering [10–12]. For group IV semiconductors such as diamond, silicon, germanium, silicon carbide, and silicon germanium, the most common dopants are acceptors from Group III or donors from Group V elements. In addition, boron, arsenic, phosphorus, and occasionally gallium have been used as dopants in these doping techniques [13–21]. In the case of controlling graphene's properties, the boron and nitrogen atoms located on the left and right of the carbon in the periodic table have been used as p-type and n-type dopants in the synthesis of graphene [22, 23]. Among many dopants for graphene, amine-based organic compounds have been used as n-type dopants to decrease the graphene work function.

Contact resistance between graphene and metal in electronic devices has limited the performance of electronic devices [20]. This means that tuning the graphene work function in electronic devices is crucial to determining the characteristics of graphene-based devices. Recently, *N,N,N′,N″*-tetraphenylethylenediamine (TPEDA) and similar amine-containing materials have been used to change the properties of graphene oxides [24–26]. However, the effects of amine-based organic compounds on graphene's properties have not yet been extensively studied. Further research is needed to elucidate the role of amine groups and their derivatives in graphene doping techniques.

In this study, we investigated the role of amine-based organic compounds with various functional groups in graphene doping. TPEDA (represented by H), which is readily available as a base material, was used as a standard dopant. Seven different types of end groups (methyl (Me), ethyl (Et), propyl (Pr), *n*-butyl (*n*-Bu), *t*-butyl (*t*-Bu), and octyl (Oc)) were prepared to check the degree of doping performance. Changes in sheet resistance (R_{sh}) and transmittance were confirmed using four-point probe technology and ultraviolet (UV) visible spectroscopy. The Raman spectra of G and 2D peak positions were measured to confirm the degree of doping in the graphene network. Core-level spectra and secondary electron cut-off spectra were identified to confirm changes in composition and work functions after organic doping using UV light emission spectroscopy (UPS) and synchrotron-radiation photoemission spectroscopy (SRPES). On the basis of various experimental data, we analyzed the doping effect of amine-based organic compounds on graphene as a function of dopant end group, and propose a possible doping mechanism.

2 Experimental Procedure

2.1 General

All reactions were conducted under an inert N_2 atmosphere. Commercially available reagents were used without further purification, unless otherwise stated. ^{1}H NMR(Nuclear Magnetic Resonance) (300 or 600 MHz) and ^{13}C NMR (75 or 150 MHz) were recorded in $CDCl_3$ as solvent, using tetramethylsilane (TMS) as an internal standard, unless otherwise stated. Chemical shifts are reported in δ units (ppm) by assigning the TMS resonance in the ^{1}H NMR spectrum as 0.00 ppm and the $CDCl_3$ resonance in the ^{13}C spectrum as 77.2 ppm. All coupling constants, J, are reported in hertz (Hz). Flash column chromatography was performed on silica gel 60, 70–230 mesh. Analytical thin-layer chromatography (TLC) was performed using Merck Kieselgel 60 F254 precoated plates with a fluorescent indicator and visualized with UV light (254 and 365 nm in wavelength) or by iodine vapor staining. The R_{sh} was measured in a standard state using a four-point probe technique (Keithley 2612A multimeter; Keithley Instruments, Solon, OH, USA). UV–visible spectra were recorded on a JASCO V-740 photo-spectrometer. Raman spectra of graphene were obtained with a Lab RAM HR (Horiba Jobin Yvon, Kyoto, Japan) at an excitation wavelength of 514.54 nm. An amine-based compound was doped on the graphene surface, and field-emission scanning electron microscopy (FESEM) was measured to confirm the surface change [27]. SRPES experiments were performed in an ultrahigh-vacuum chamber (base pressure of ~ 10^{-10} Torr) in the 4D beamline, equipped with an electron analyzer and a heating element, at the Pohang Acceleration Laboratory. The onset of photoemission, corresponding to the vacuum level at the surface of the graphene, was measured using an incident photon energy of 250 eV with a negative bias on the sample. The results were corrected for charging effects by using Au 4f as an internal reference.

2.2 Synthesis Scheme

To bis(dibenzylideneacetone)palladium(0) (125 mg, 0.217 mmol), (±)-2,2′-bis(diphenylphosphino)-1,1′-binaphthalene ((±)-BINAP) (270 mg, 0.434 mmol), sodium *tert*-butoxide (4.22 g, 43.9 mmol) in a two-neck round-bottom flask under nitrogen atmosphere was added 1,4-dioxane (50.0 mL) and bromoarene (43.5 mmol). After stirring for 1 h at room temperature, ethylenediamine (0.50 mL, 7.25 mmol) was added, and the reaction mixture was heated at reflux for 72 h. The reaction mixture was cooled to room

temperature; diluted with chloroform (200.0 mL); washed with 1% aqueous HCl, water, and brine three times; and dried over $MgSO_4$. The resulting solution was concentrated under vacuum to afford the crude product that was further purified by recrystallization, column chromatography, or a simple washing.

2.2.1 *N,N,N′,N′*-tetraphenylethylenediamine (N1)

N,N,N′,N′-tetraphenylethylenediamine (N1) was prepared by the reaction of bis(dibenzylideneacetone) palladium(0) (125 mg, 0.217 mmol), (±)-BINAP (270 mg, 0.434 mmol), sodium *tert*-butoxide (4.22 g, 43.9 mmol), bromobenzene (4.57 mL, 43.5 mmol), and ethylenediamine (0.50 mL, 7.25 mmol). The crude product was purified by recrystallization (CH_2Cl_2:*n*-hexane = 1:3) to afford **N1** (2.02 g, 76.5%) as a clear needle-shaped crystal: mp 115–116 °C; TLC R_f 0.72 (Et_2O:*n*-hexane = 1:1); ^{1}H-NMR (600 MHz, $CDCl_3$) δ 7.23 (t, J = 7.87 Hz, 8H), 6.97–6.92 (m, 12H), 3.99 (s, 4H); ^{13}C-NMR(150 MHz, $CDCl_3$) δ 147.63 (4C), 129.34 (8C), 121.50 (4C), 120.80 (8C), 49.63 (2C).

2.2.2 *N,N,N′,N′*-tetrakis(4-methylphenyl)ethylenediamine (N2)

N,N,N′,N′-tetrakis(4-methylphenyl) ethylenediamine (N2) was prepared by the reaction of bis (dibenzylideneacetone) palladium(0) (125 mg, 0.217 mmol), (±)-BINAP (270 mg, 0.434 mmol), sodium *tert*-butoxide (4.22 g, 43.9 mmol), 1-bromo-4-methylbenzene (5.32 mL, 43.5 mmol), and ethylenediamine (0.50 mL, 7.25 mmol). The crude product was purified by column chromatography to afford **N2** (2.15 g, 70.4%) as a white powder: mp 141 °C; TLC R_f 0.80 (Et_2O:*n*-hexane = 1:5); ^{1}H-NMR (300 MHz, $CDCl_3$) δ 7.02 (d, J = 8.49 Hz, 8H), 6.83 (d, J = 8.49 Hz 8H), 3.89 (s, 4H), 2.27 (s, 12H); ^{13}C-NMR(150 MHz, $CDCl_3$) δ 145.60 (4C), 130.55 (4C), 129.82 (8C), 120.70 (8C), 49.73 (2C), 20.59 (4C).

2.2.3 *N,N,N′,N′*-tetrakis(4-ethylphenyl)ethylenediamine (N3)

N,N,N′,N′-tetrakis(4-ethylphenyl)ethylenediamine (N3) was prepared by the reaction of bis(dibenzylideneacetone) palladium(0) (125 mg, 0.217 mmol), (±)-BINAP (270 mg, 0.434 mmol), sodium *tert*-butoxide (4.22 g, 43.9 mmol), 1-bromo-4-ethylbenzene (5.97 mL, 43.5 mmol), and ethylenediamine (0.50 mL, 7.25 mmol). The crude product was purified by column chromatography to afford **N3** (1.87 g, 54.2%)) as a white powder: mp 74 °C; TLC R_f 0.77 (Et_2O:*n*-hexane = 1:5); ^{1}H-NMR (600 MHz, $CDCl_3$) δ 7.06 (d, J = 8.57 Hz, 8H), 6.86 (d, J = 8.57 Hz 8H), 3.93 (s, 4H), 2.60 (q, J = 7.60 Hz, 8H), 1.23 (t, J = 7.60 Hz, 12H); ^{13}C-NMR(150 MHz, $CDCl_3$) δ 145.72 (4C), 137.00 (4C), 128.57 (8C), 120.66 (8C), 49.73 (2C), 28.06 (4C), 15.68 (4C).

2.2.4 *N,N,N′,N′*-tetrakis(4-propylphenyl)ethylenediamine (N4)

N,N,N′,N′-tetrakis(4-propylphenyl)ethylenediamine (N4) was prepared by the reaction of bis(dibenzylideneacetone) palladium(0) (125 mg, 0.217 mmol), (±)-BINAP (270 mg, 0.434 mmol), sodium *tert*-butoxide (4.22 g, 43.9 mmol), 1-bromo-4-propylbenzene (6.75 mL, 43.5 mmol), and ethylenediamine (0.50 mL, 7.25 mmol). The crude product was purified by column chromatography to afford **N4** (1.86 g, 48.1%) as a white powder: mp 63 °C; TLC R_f 0.87 (Et_2O:*n*-hexane = 1:5); ^{1}H-NMR (600 MHz, $CDCl_3$) δ 7.02 (d, J = 8.56 Hz, 8H), 6.84 (d, J = 8.56 Hz 8H), 3.92 (s, 4H), 2.52 (t, J = 7.64 Hz, 8H), 1.61 (sextet, J = 7.46 Hz, 8H), 0.95 (t, J = 7.30 Hz, 12H); ^{13}C-NMR(150 MHz, $CDCl_3$) δ 145.72 (4C), 135.45 (4C), 129.18 (8C), 120.56 (8C), 49.69 (2C), 37.30 (4C), 24.65 (4C), 13.86 (4C).

2.2.5 *N,N,N′,N′*-tetrakis(4-butylphenyl)ethylenediamine (N5)

N,N,N′,N′-tetrakis(4-butylphenyl)ethylenediamine (N5) was prepared by the reaction of bis(dibenzylideneacetone) palladium(0) (125 mg, 0.217 mmol), (±)-BINAP (270 mg, 0.434 mmol), sodium *tert*-butoxide (4.22 g, 43.9 mmol), 1-bromo-4-butylbenzene (11.45 mL, 43.5 mmol), and ethylenediamine (0.50 mL, 7.25 mmol). The crude product was purified by a facile precipitation column chromatography (ethyl acetate:*n*-hexane = 1:20) to afford **N5** (1.46 g, 34.2%) as a clear needle-shaped crystal: mp 49 °C; TLC R_f 0.79 (Et_2O:*n*-hexane = 1:9); ^{1}H-NMR (600 MHz, $CDCl_3$, δ) 7.02 (d, J = 8.55 Hz, 8H), 6.84 (d, J = 8.55 Hz, 8H), 3.92 (s, 4H), 2.55 (t, J = 7.74 Hz, 8H), 1.58 (quintet, J = 7.46 Hz, 8H), 1.36 (sextet, J = 7.43 Hz, 8H), 0.94 (t, J = 7.36 Hz, 12H); ^{13}C-NMR(150 MHz, $CDCl_3$, δ) 145.66 (4C), 135.63 (4C), 129.10 (8C), 120.56 (8C), 49.66 (2C), 34.86 (4C), 33.77 (4C), 22.36 (4C), 13.98 (4C).

2.2.6 *N,N,N′,N′*-tetrakis(4-(*tert*-butyl)phenyl) ethylenediamine (N6)

N,N,N′,N′-tetrakis(4-(*tert*-butyl)phenyl) ethylenediamine (N6) was prepared by the reaction of bis(dibenzylideneacetone)palladium(0) (125 mg, 0.217 mmol), (±)-BINAP (270 mg, 0.434 mmol), sodium *tert*-butoxide (4.22 g, 43.9 mmol), 1-bromo-4-*tert*-butylbenzene (7.71 mL, 43.5 mmol), and ethylenediamine (0.50 mL, 7.25 mmol). The crude product was purified by column chromatography to afford **N6** (1.40 g, 32.8%) as a white powder:

mp 228 – 229 °C; TLC R_f 0.78 (Et_2O:*n*-hexane = 1:9); ^{1}H-NMR (600 MHz, $CDCl_3$) δ 7.24 (d, J = 8.66 Hz, 8H), 6.87 (d, J = 8.66 Hz 8H), 3.94 (s, 4H), 1.31 (s, 36H); ^{13}C-NMR(150 MHz, $CDCl_3$) δ 145.26 (4C), 143.86 (4C), 126.02 (8C), 120.19 (8C), 49.62 (2C), 34.12 (4C), 31.47 (12C).

2.2.7 *N,N,N′,N′*-tetrakis(4-octylphenyl)ethylenediamine (N7)

N,N,N′,N′-tetrakis(4-octylphenyl)ethylenediamine (N7) was prepared by the reaction of bis(dibenzylideneacetone) palladium(0) (125 mg, 0.217 mmol), (±)-BINAP (270 mg, 0.434 mmol), sodium *tert*-butoxide (4.22 g, 43.9 mmol), 4-octyl-1-bromobenzene (10.3 mL, 43.5 mmol), and ethylenediamine (0.50 mL, 7.25 mmol). The crude product was purified by column chromatography to afford **N7** (1.43 g, 24.4%) as a white powder: mp 39 °C; TLC R_f 0.47 (CH_2Cl_2:*n*-hexane = 1:3); ^{1}H-NMR (600 MHz, $CDCl_3$) δ 7.02 (d, J = 8.53 Hz, 8H), 6.83 (d, J = 8.53 Hz 8H), 3.91 (s, 4H), δ 2.53 (t, J = 7.76 Hz, 8H), δ 1.59 (quintet, J = 7.55 Hz, 8H), 1.30 (m, 30H), δ 0.88 (t, J = 7.06 Hz, 12H); ^{13}C-NMR(150 MHz, $CDCl_3$) δ 145.65 (4C), 135.68 (4C), 129.08 (8C), 120.55 (8C), 49.65 (2C), 35.20 (4C), 31.90 (4C), 31.63 (4C), 29.51 (4C), 29.37 (4C), 29.28 (4C), 22.67 (4C), 14.10 (4C).

2.3 Preparation of Graphene Film

Graphene samples were grown on a 25-μm-thick copper foil in a quartz tube furnace, using a CVD method involving methane (CH_4) and hydrogen (H_2) gas. Under a vacuum of 90 mTorr, the furnace was heated without a gas flow for 30 min. Before the growth of graphene, the copper foil was preheated at 950 °C for 30 min. To obtain a large single-crystal copper surface, H_2 gas was supplied to the furnace under a vacuum of 150 mTorr at a rate of 33 cm^3/min (sccm). After the preheating step, a gas mixture of CH_4 and H_2 was supplied at a ratio of 200 sccm/33 sccm under ambient conditions for 10 min to synthesize the graphene. After 10 min of growth, the furnace was cooled to room temperature at a rate of 10–15 °C/min, under a H_2 flow of 33 sccm. Poly(methyl methacrylate) (PMMA) was then spin-coated onto the graphene, and the PMMA-coated foil was heated on a hot plate at 180 °C for 1 min, after which O_2 plasma was used to etch the graphene on the other side of the copper foil. The sample was then immersed in a ferric chloride (1 M $FeCl_3$) bath at room temperature for 12–18 h to etch away the copper foil. The remaining sample was carefully dipped into a deionized water bath approximately 7–9 times to remove any residual etchant. The graphene sheets were then transferred onto an arbitrary substrate. The PMMA was removed by immersion in an acetone bath at 50 °C for 30 min after the graphene layer had completely adhered to the target substrate.

2.4 Doping Procedures

After the graphene sheets were transferred to a glass slide or a Si/SiO_2 wafer substrate, the sample was placed on the spin-coater. The chemical structures of the purchased TPEDA and synthesized amine-based organic compounds with seven different functional groups (H, Me, Et, Pr, *n*-Bu, *t*-Bu, and Oc) and synthetic methods are shown in Fig. 1. The amine-based organic compounds were separately dissolved in chloroform at three different concentrations: 10, 20, and 40 mM (i.e., a total of 21 different solutions were prepared). Then, 1 mL of each of the solutions was pipetted on top of the transferred graphene substrates, allowed to stand for 1 min, and then spun at 2500 rpm for 1 min. Finally, the samples were annealed at 150 °C on a hot plate for 2 min to evaporate the solvent.

3 Results and Discussion

3.1 Material Properties

Figure 2a shows the change in the transmittance spectra of graphene doped with different materials. The transmittance of pristine graphene (P-G) without any dopant was 97% at 550 nm. This is similar to the results shown in previous reports [28, 29]. The transmittance values of the graphene spin-coated with different amine-based organic compounds were 95, 94.8, 83.3, 74, 73, and 68.8% at 550 nm for the H, Me, Et, Pr, *n*-Bu, *t*-Bu, and Oc samples. This indicates that the organic compound doping on the graphene surface reduces the transmittance values regardless of the ending functional group. Figure 2b shows the change of R_{sh} as a

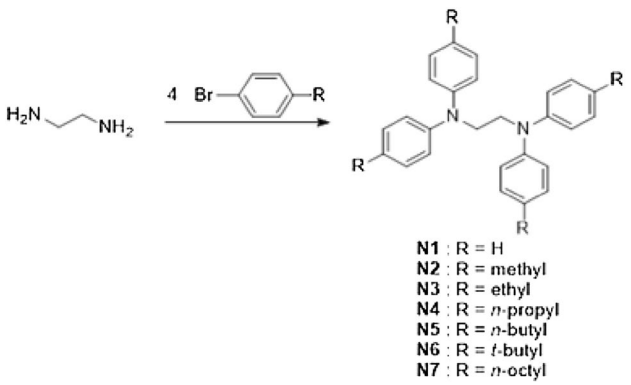

Fig. 1 Synthesis scheme for amine-based compounds. Methyl, ethyl, *n*-propyl, *n*-butyl, *t*-butyl, and *n*-octyl were used as substituents for N1, N2, N3, N4, N5, N6, and N7, respectively

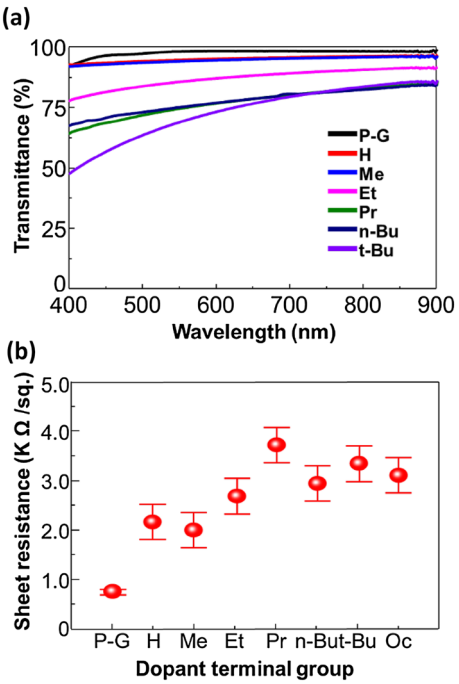

Fig. 2 **a** The transmittance values decreased and the sheet resistance value increased after doping. The transmittance of pristine graphene at 550 nm was found to be approximately 97%. **b** Sheet resistance after doping with amine-based compounds at a concentration of 20 mM

function of ending functional group. It changed from 700 to 2150, 1920, 2600, 3700, 2900, 3350, and 3080 Ω/sq after doping with H, Me, Et, Pr, *n*-Bu, *t*-Bu, and Oc samples, respectively. The R_{sh} values of all samples were higher than the R_{sh} value of P-G regardless of the doping material. Graphene has been reported to have p-type properties. Thus, the change in R_{sh} signifies n-type doping of graphene or the depletion of holes [7]. It is considered that electrons have moved spontaneously from the amine-based compounds to the graphene sheets. The reason for this is that the nitrogen atom is not a planar structure but a triangular structure, and a lone pair exists. The lone pair acts as a nucleophile to share electrons with graphene or to bind electrons to graphene, which improves the electrical properties of the graphene and increases electron mobility [30–32].

Figure 3 shows the Raman spectra of P-G and graphene samples coated with amine-based compounds. The D peak (1350 cm^{-1}), G peak (1580 cm^{-1}), and 2D peak (2700 cm^{-1}) of the Raman spectra are related to disorder, doping state, and number of graphene layers, respectively [33, 34]. The vertical dashed line in Fig. 4 shows the position of the G and 2D peaks in the P-G sample. This value is similar to the previously reported value. For a graphene sample doped with an amine-based compound, the position of the G peak shifted to a higher value, and the 2D peak position shifted to a lower value regardless of the dopant material. When

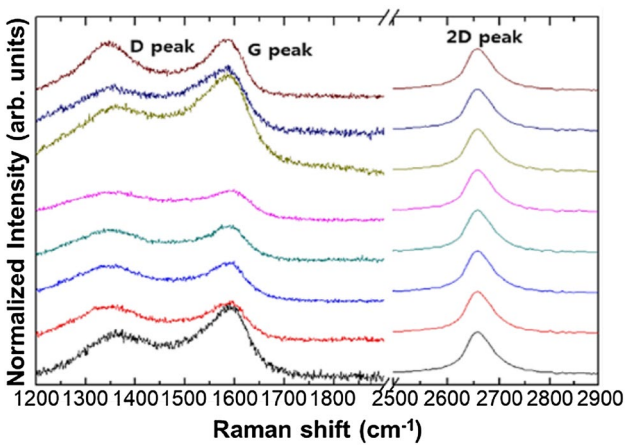

Fig. 3 Raman spectroscopy analysis of pristine graphene sheets and sheets doped with different amine compounds. Wide peak investigation includes the D, G, and 2D bands

the amine-based compound was doped into graphene, the intensity ratio of the 2D-band peak to the G peak and the 2D peak varied from 1:6 to 1:2. The 2D peak was red-shifted after doping compared with graphene before doping, and its intensity decreased. The G peak increased in intensity and peaked, because graphene becomes richer in electrons and holes, resulting in a narrower G-peak line width and larger intensity [35].

To confirm the presence of an amine-based compound, graphene samples were opened to electron-beam radiation for 10 s at 5 kV. An FESEM image of the P-G and doped graphene after the electron-beam irradiation is shown in Fig. 4. Prior to electron-beam irradiation, P-G showed precise characteristics of grains and PMMA residues. Between the P-G and doped graphene, patterns not shown in P-G appeared in the doped graphene. An FESEM image of P-G and doped graphene after electron beam processing is shown

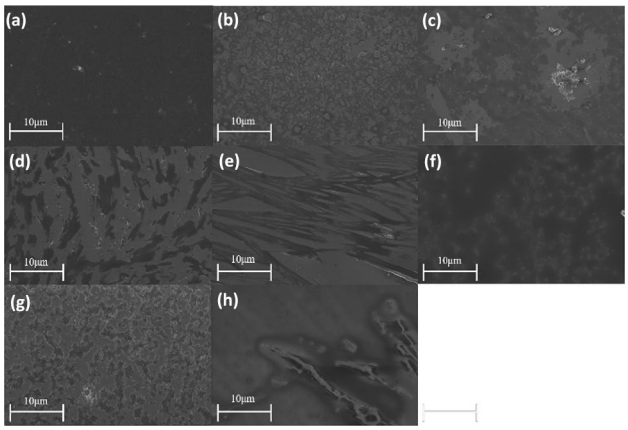

Fig. 4 FESEM images of **a** P-G and **b** H-, **c** Me-, **d** Et-, **e** Pr-, **f** n-Bu-, **g** t-Bu-, and **h** Oc-doped graphene exposed to 5-kV electrons for 10 s

in Fig. 4. There is a difference between the images of P-G and doped graphene. Different patterns appeared for each doping material. This result confirms that the amine-based compound is well coated on the surface of the graphene. This result indicates that the organic compound is actually well spread on the surface of the graphene.

Figure 5a shows the C 1s spectra of P-G and graphene coated with several amine-based organic compounds with a 20 mM concentration. The C 1s peak of P-G is composed of C=C bond at 284.7 eV, C–O bonds at 287.3 eV, carbonyl bond (C=O) at 289 eV, and a π–π bond at 291.8 eV, indicating that some oxide groups exist in P-G even though the graphene was synthesized by CVD [36]. This seems to have arisen from the hot-acetone-bath cleaning process, as already known from other studies [6]. We analyzed each sample using SRPES to better understand the surface changes of P-G due to amine-based-compound doping. Figure 5a shows the C 1s core-level spectra when each material is doped with 20-mM concentration. Four peaks appear in the binding energy region corresponding to the structural elements of the groups C=C (284.5 eV), CN (285.9 eV), CO (287.2 eV), and C=O (289 eV). C=O bonds or C–O bonds were weak or strong in P-G or other doping samples because P-G is bonded by exposure to air, and the length of the functional group is long in Oc, and the peak is not formed because C is not bonded [37]. Figure 5b shows N 1s core-level spectra when each material is doped with 20 mM concentration. No nitrogen peak occurred in the case of P-G. Two peaks appeared in the binding energy region of the N–C (399.5 eV) and N–C–H (401.8 eV) groups. As the functional group of the doping material becomes complicated, the N–C peak appears stronger. This result confirms that each amine-based compound is properly doped in P-G.

Figure 6a shows the UPS spectra of P-G and graphene with 20-mM amine-based organic compounds. The work-function values were 4.43 eV for PG and 4.43, 4.21, 4.16, 4.14, 4.04, 3.89, and 4.06 eV for H, Me, Et, Pr, *n*-Bu, *t*-Bu, and Oc, respectively. In the case of amine-based organic compounds, it is expected that the work function will decrease because the terminal group cannot completely cover the surface because of the steric hindrance. Therefore, the basic work-function value is thought to come from

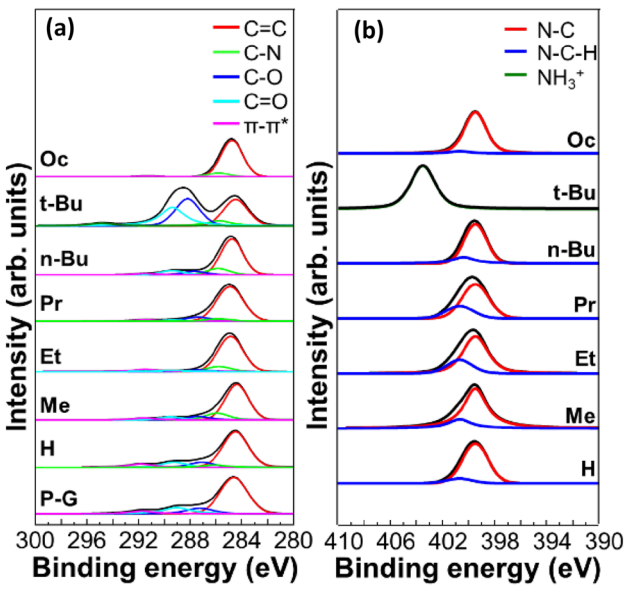

Fig. 5 SRPES analysis of pristine graphene sheet and sheets doped with different amine compounds: **a** C 1s core-level spectra, **b** N 1s core-level spectra. No nitrogen peak occurred in the case of pristine graphene

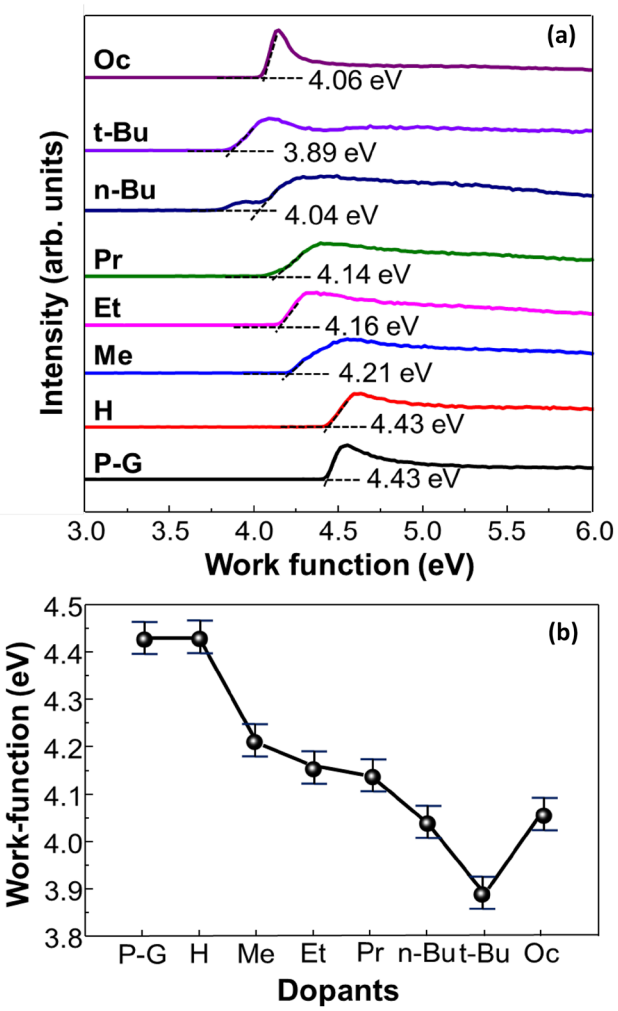

Fig. 6 UPS spectra and work function: **a** UPS spectra of graphene doped with different amine compounds. The onset of the secondary-electron cutoff energy was determined by extrapolating two straight lines from the background and the shoulders in the spectra. **b** Summary of the variations of the work functions of doped graphene sheets as functions of the type of dopant. It is confirmed that the charge transfer resistance significantly decreased when the graphene layer was transferred on the substrate

the graphene sample [38]. Figure 6b is a graphical representation of the work function values calculated in Fig. 6a. This graph shows the work function changes of amine-based organic compounds in chloroform, a nonpolar solvent. The work function was changed because of steric hindrance of the end group of the amine-based organic compounds; the largest change was observed in the *t*-Bu sample with the most steric hindrance [39, 40].

4 Conclusions

Doping efficiency of doped amine-based compounds on graphene sheets was confirmed by various experiments. It was confirmed that the R_{sh} value increased from 550 nm to 68.8% P-G, reaching 95% while the amine compound was coated on the graphene sheet. We also confirmed that the 2D peak in the Raman spectrum was blue-shifted, and the intensity change of the G peak was also confirmed. This result indicates that the amine compound is doped in the graphene sheet and used as an n-type dopant. In the SRPES spectra, confirmation of the C 1s peak and N 1s peak confirmed that the amine compound was properly doped to the surface. It was confirmed that the work function changed from 4.43 eV to 3.89 eV for the P-G sample. The greatest change was observed in the *t*-bu sample. The *t*-bu sample exhibited the largest doping effect, due to the large steric hindrance, compared with the other samples, resulting in large changes in the work function and Raman, SRPES, and R_{sh} results. Thus, we found that the steric hindrance of amine-based compound functional groups has a major impact on the n-type doping and hole depletion of graphene.

Acknowledgements This research was supported by a National Research Foundation of Korea (NRF) grant funded by the Korean government (MSIP) (Nos. 2018R1A4A1022647); and this research was supported by the Chung-Ang University Research Scholarship Grants in 2015.

References

1. Geim, A.K.: Graphene: status and prospects. Science **324**, 1530–1534 (2009)
2. Du, X., Skachko, I., Barker, A., Andrei, E.Y.: Approaching ballistic transport in suspended graphene. Nat. Nanotechnol. **3**, 491–495 (2008)
3. Novoselov, K.S., Jiang, Z., Zhang, Y., Morozov, S., Stormer, H.L., Zeitler, U., Maan, J., Boebinger, G., Kim, P., Geim, A.K.: Room-temperature quantum hall effect in graphene. Science **315**, 1379 (2007)
4. Obraztsov, A., Obraztsova, E.A., Tyurnina, A.V., Zolotukhin, A.: Chemical vapor deposition of thin graphite films of nanometer thickness. Carbon **45**, 2017–2021 (2007)
5. Im, H., Kim, J.H.: Thermal conductivity of a graphene oxide–carbon nanotube hybrid/epoxy composite. Carbon **50**, 5429–5440 (2012)
6. Kwon, K.C., Son, H.J., Hwang, Y.H., Oh, J.H., Lee, T.-W., Jang, H.W., Kwak, K., Park, K., Kim, S.Y.: Effect of amine-based organic compounds on the work-function decrease of graphene. J. Phys. Chem. C **120**, 1309–1316 (2016)
7. Bae, S., Kim, H.K., Lee, Y.B., Xu, X., Park, J.-S., Zheng, Y., Balakrishnan, J., Lei, T., Kim, H.R., Song, Y.I., Kim, Y.-J., Kim, K.S., Ozilmaz, B., Ahn, J.H., Hong, B.H., Iijima, S.: Roll-roll production of 30-inch graphene films for transparent electrodes. Nat. Nanotechnol. **5**, 574–578 (2010)
8. Kim, K.S., Zhao, Y., Jang, H., Lee, S.Y., Kim, J.M., Kim, K.S., Ahn, J.-H., Kim, P., Choi, J.-Y., Hong, B.H.: Large-scale pattern growth of graphene films for stretchable transparent electrodes. Nature **457**, 706–710 (2009)
9. Li, X., Cai, W., An, J., Kim, S., Nah, J., Yang, D., Piner, R., Velamakanni, A., Jung, I., Tutuc, E., Banergee, S.K., Colombo, L., Ruoff, R.S.: Large-area synthesis of high-quality and uniform graphene films on copper foils. Science **324**, 1312–1314 (2009)
10. Kwon, K.C., Choi, K.S., Kim, B.J., Lee, J.-L., Kim, S.Y.: Work-function decrease of graphene sheet using alkali metal carbonates. J. Phys. Chem. C **116**, 26586–26591 (2012)
11. Kwon, K.C., Choi, K.S., Kim, C., Kim, S.Y.: Effect of transition-metal chlorides on graphene properties. Phys. Status Solidi a **211**, 1794–1800 (2014)
12. Kwon, K.C., Choi, K.S., Kim, S.Y.: Increased work function in few-layer graphene sheets via metal chloride doping. Adv. Funct. Mater. **22**, 4724–4731 (2012)
13. Kwon, K., Kim, B.J., Lee, J.-L., Kim, S.Y.: Role of ionic chlorine in the thermal degradation of metal chloride-doping graphene sheets. J. Mater. Chem. C **1**, 253–259 (2013)
14. Christodoulou, C., Giannakopoulos, A., Nardi, M.V., Ligorio, G., Oehzelt, M., Chen, L., Pasquali, L., Timpel, M., Giglia, A., Nannarone, S., Norman, P., Parvez, K., Mullen, K., Deljonne, D., Koch, N.: Tuning the work function of graphene-on-quartz with a high weight molecualr acceptor. J. Phys. Chem. C **118**, 4784–4790 (2014)
15. Gholizadeh, R., Yu, Y.-X.: Work function of pristine and heteroatom-doped graphenes under different external electric fields:an ab initio DFT study. J. Phys. Chem. C **118**, 28274–28282 (2014)
16. Yu, Y.-X.: A dispersion-corrected DFT study on adsorption of battery active materials anthraquinone and its derivatives on monolayer graphene and h-BN. J. Mater. Chem. A **2**, 8910–8917 (2014)
17. Yu, Y.-X.: Binding energy and work function of organic electrode materials phenanthraquinone, pyromellitic dianhydride and their derivatives adsorbed on graphene. Appl. Mater. Interfaces **6**, 16267–16275 (2014)
18. Basko, D.M., Piscanec, S., Ferrari, A.C.: Electron–electron interactions and doping dependence of the two-phonon Raman intensity in graphene. Phys. Rev. B **80**, 165413 (2009)
19. Dong, X., Fu, D., Fang, W., Shi, Y., Chen, P., Li, L.-J.: Doping single-layer graphene with aromatic molecules. Small **5**(12), 1422 (2009)
20. Chen, Z., Santoso, I., Wang, R., Xie, L.F., Mao, H.Y., Huang, H., Wang, Y.Z., Gao, X.Y., Chen, Z.K., Ma, D., Wee, A.T.S., Chen, W.: Surface transfer hole doping of epitaxial graphene using MoO_3 thin film. Appl. Phys. Lett. **96**, 213104 (2010)
21. Han, C., Lin, J., Xiang, D., Wang, C., Wang, L., Chen, W.: Improving chemical vapor deposition graphene conductivity using molybdenum trioxide: an in-situ field effect transistor study. Appl. Phys. Lett. **103**, 263117 (2013)
22. Panchakarla, L., Subrahmanyam, K., Saha, S., Govindaraj, A., Krishnamurthy, H., Waghmare, U., Rao, C.N.: Synthesis,

structure, and properties of boron- and nitrogen-doped graphene. Adv. Mater. **21**, 4726–4730 (2009)
23. Hwang, J.O., Park, J.S., Choi, D.S., Kim, J.Y., Lee, S.H., Lee, K.E., Kim, Y.-H., Song, M.H., Yoo, S., Kim, S.O.: Workfunction-tunable, N-doped reduced graphene transparent electrodes for high-performance polymer light-emitting diodes. ACS Nano **6**, 159–167 (2011)
24. Deng, Y., Li, Y., Dai, J., Lang, M., Huang, X.: An efficient way to functionalize graphene sheets with presynthesized polymer via ATNRC chemistry. J. Polym. Chem. **49**, 1582–1590 (2011)
25. Ren, L., Huang, S., Zhang, C., Wang, R., Tjiu, W.W., Liu, T.: Functionalization of graphene and grafting of temperature-responsive surfaces from graphene by ATRP "on water". J. Nanopart. Res. **14**, 940 (2012)
26. Shanmugharaj, A., Yoon, J., Yang, W., Ryu, S.H.: Synthesis, characterization, and surface wettability properties of amine functionalized graphene oxide films with varying amine chain lengths. J. Colloid Interface Sci. **401**, 148 (2013)
27. Kim, C., Yoon, M.-J., Hong, S.H., Park, M., Park, K., Kim, S.Y.: Aromatic substituents for prohibiting side-chain packing and π–π stacking in tin-cored tetrahedral stilbenoids. Electron. Mater. Lett. **12**, 388–398 (2016)
28. Song, S.M., Park, J.K., Sul, O.J., Cho, B.J.: Determination of work function of graphene under a metal electrode and its role in contact resistance. Nano Lett. **12**, 3887–3892 (2012)
29. Shi, Y., Kim, K.K., Reina, A., Hofmann, M., Li, L.-J., Kong, J.: Work function engineering of graphene electrode *via* chemical doping. ACS Nano **4**, 2689–2694 (2010)
30. Jo, I., Kim, Y., Moon, J., Park, S., Moon, J.S., Park, W.B., Lee, J.S., Hong, H.: Stable n-type doping of graphene *via* high-molecular-weight ethylene amines. Phys. Chem. Chem. Phys. **17**, 29492–29495 (2015)
31. Ishikawa, R., Bando, M., Morimoto, Y., Sandhu, A.: Doping graphene films via chemically mediated charge transfer. Nano Res Lett **6**, 111 (2011)
32. Lee, W.H., Suk, J.W., Lee, J., Hao, Y., Park, J., Yang, J.W., Ha, H.-W., Murali, S., Chou, H., Akinwande, H., Kim, K.S., Ruoff, R.S.: Simultaneous transfer and doping of CVD-grown graphene by fluoropolymer for transparent conductive films on plastic. ACS Nano **6**, 1284–1290 (2012)
33. Podila, R., Rao, R., Tsuchikawa, R., Ishigami, M., Rao, A.M.: Raman spectroscopy of folded and scrolled graphene. ACS Nano **6**, 5784–5790 (2012)
34. Sun, T., Wang, Z., Shi, Z., Ran, G., Xu, W., Wang, Z., Li, Y., Dai, L., Qin, G.: Multilayered graphene used as anode of organic light emitting devices. Appl. Phys. Lett. **96**, 55 (2010)
35. Ferrari, A.C.: Raman spectroscopy of graphene and graphite: Disorder, electron–phonon coupling, doping and nonadiabatic effects. Solid State Commun. **143**, 47–57 (2007)
36. Kwon, K.C., Son, P.K., Kim, S.Y.: Ion beam irradiation of few-layer graphene and its application to liquid crystal cells. Carbon **67**, 352–359 (2014)
37. Oh, J.H., Choi, G.J., Kwon, K.C., Bae, S.-R., Jang, H.W., Gwag, J.S., Kim, S.Y.: Ion-beam-irradiated CYTOP-transferred graphene for liquid crystal cells. Electron. Mater. Lett. **13**, 277–285 (2017)
38. Zafar, Z., Ni, Z.H., Wu, X., Shi, Z.X., Nan, H.Y., Bai, J., Sun, L.T.: Evolution of raman spectra in nitrogen doped graphene. Carbon **61**, 57–62 (2013)
39. Ramanathan, T., Fisher, F., Ruoff, R., Brinson, L.C.: Amino-functionalized carbon nanotubes for binding to polymers and biological systems. Chem. Mater. **17**, 1290–1295 (2005)
40. Jansen, R., Bekkum, H.V.: XPS of nitrogen-containing functional groups on activated carbon. Carbon **33**, 1021–1027 (1995)